Journal of Natural Gas Science and Engineering 99 (2022) 104453

Contents lists available at ScienceDirect

Journal of Natural Gas Science and Engineering

journal homepage: www.elsevier.com/locate/jngse

Effect of overburden spatial variability on field-scale geomechanical modeling of potential CO_2 storage site Smeaheia, offshore Norway

Md Jamilur Rahman [a,*], Manzar Fawad [a], Jung Chan Choi [b], Nazmul Haque Mondol [a,b]

[a] Department of Geosciences, University of Oslo (UiO), Sem Saelands vei 1, 0371, Oslo, Norway
[b] Norwegian Geotechnical Institute (NGI), Sognsveien 72, 0806, Oslo, Norway

ARTICLE INFO

Keywords:
Smeaheia
3D field-scale geomechanical model
Surface deformation
One-way coupling
Finite element method
Overburden
Spatial variability

ABSTRACT

Although geological CO_2 sequestration is an essential solution for reducing anthropogenic carbon dioxide from the atmosphere, the method needs critical evaluation of injection-induced mechanical risks for safe and reliable CO_2 storage. 3D field-scale geomechanical modeling is a preeminent solution for assessing mechanical risks of subsurface geological CO_2 storage. However, data scarcity of seals and overburden rocks might limit building the 3D field-scale geomechanical model. This study focuses on seismic data-derived 3D field-scale geomechanical modeling of potential CO_2 storage site Smeaheia, offshore Norway. The geomechanical properties inverted from seismic data are resampled in the 3D grid to consider spatial variabilities of seal and overburden rock properties. This method allows us to investigate the effect of overburden rock spatial variability imposed in seismic data on the 3D geomechanical model of Smeaheia. The model was built in Petrel-2019, while the one-way geomechanical simulation is iterated using the finite element method. Simplified constant overburden property models are also constructed to analyze the sensitivity of the overburden rock properties. The results reveal that the seismic data-driven spatially distributed overburden properties model workflow used in this study is a convenient and robust solution for 3D field-scale geomechanical modeling. The maximum vertical estimation of rock deformation is doubled in the simplified (isotropic) overburden rock property model compared to the new spatially variable (anisotropic) overburden rock property model. The Mohr-Coulomb failure envelope reveals that the new modeling approach is less prone to failure than the simplified (isotropic) model, which might influence the project decision. Moreover, our study demonstrates the importance of considering the spatial variability of overburden rock properties in building the 3D field-scale geomechanical model.

1. Introduction

Geological sequestration of anthropogenic CO_2 (CCS) into saline aquifers or depleted hydrocarbon reservoirs is one of the many solutions to achieve the Paris Climate Accords to keep the average global temperature rise well below 2 °C by 2050. According to NPD CO_2 Atlas (2014), the CO_2 storage capacity of the Norwegian Continental Shelf (NCS) is significant, where the Norwegian government and industries already show interest in the gigaton level of CO_2 storage (i.e., Northern lights project under the Longship). The phase 1 plan for this project is to capture, transport, inject and store up to 1.5 MT of CO_2 per year, while in the future, the project will store up to 5 MT of CO_2 per year based on the market demand from the large CO_2 emitters across Europe (Northern Lights project). However, any CCS project needs critical evaluation of injection-related risks (3D field-scale geomechanical modeling) for safe, reliable, and permanent geological storage.

Injecting CO_2 into saline aquifer changes the fluid saturation that results in a local disturbance in pressure and temperature and influences the mechanical behavior of the reservoir, cap, and overburden rocks. The potential geomechanical consequences would be the flexure of the top-seal and overburden, reactivation of existing faults, induced share failure, formation of new fracture and faults, changes in porosity within the reservoir, etc. (Hawkes et al., 2005; Herwanger and Koutsabeloulis, 2011; Rutqvist et al., 2008, 2007; Soltanzadeh and Hawkes, 2008; Streit and Hillis, 2004, Fig. 1). Therefore, evaluating CO_2 injection-related geomechanical risks is essential for reliable and successful CCS projects like Smeaheia and Longship.

The reliability of the CCS project depends on seal integrity, which includes caprock effectiveness and fault sealing potential (Chiaramonte et al., 2015; Park et al., 2020; Rahman et al., 2020, 2021; Rutqvist et al.,

* Corresponding author.
E-mail address: m.j.rahman@geo.uio.no (M.J. Rahman).

https://doi.org/10.1016/j.jngse.2022.104453
Received 18 November 2021; Received in revised form 26 December 2021; Accepted 28 January 2022
Available online 4 February 2022

2007; Skurtveit et al., 2018). Generally, the top seal consists of fine-grained rocks with a significantly small pore throat radius and exceptionally high capillary entry pressure. Watts (1987) introduced the concept as hydraulic seals, i.e., seals where the capillary entry pressure is so high that seal breach only occurs due to fracturing (i.e., shear failure) of the caprock (Ingram et al., 1997). Therefore, assessment of the potential flexure of the top seal and overburden rocks becomes important. The injected CO_2 into the saline aquifer will change the effective stress (i.e., principal stress minus pore pressure) and influence the mechanical deformation of rock and failure (Verdon et al., 2013). This process may lead to enormous rock deformation, such as the seafloor heave illustrated in Fig. 1. The elastic behavior of pore fluid under the drainage condition (i.e., poroelasticity) might influence the mechanical behavior and stress path within the reservoirs (Addis, 1997; Grasso, 1992; Hillis, 2001; Segall, 1989), which also indirectly affect the above cap and overburden rocks. Additional processes such as hydraulic aperture evolution, hydrological property changes, effective stress induction, and mechanical strength degradation can influence the effective stress (Park et al., 2020; Rutqvist et al., 2007), leading to different caprock and overburden deformation.

During drilling a well, there has been good coverage of data (i.e., cores, wireline logs, pressure data, etc.) acquired in the reservoir section. However, the caprock and overburden sections have mostly been ignored to collect data. This data gap is reflected in most geomechanical modeling works, where simple assumptions are used for overburden rock property evaluation (i.e., Fischer and Henk, 2013; Fokker et al., 2011; Grollimund and Zoback, 2003; Mandal et al., 2021; Newell et al., 2017; Olden et al., 2014; Ouellet et al., 2011; Tenthorey et al., 2013; Vidal-Gilbert et al., 2010). However, the effectiveness of 3D field-scale geomechanical modeling in rock deformation and failure is proven and published by several authors to evaluate the influence of CO_2 injections and gas storage projects worldwide. For instance, a 3D geomechanical model building and calibrating workflow proposed by Fischer and Henk (2013) using a gas reservoir in the North German Basin; while Vidal-Gilbert et al. (2010) and Tenthoreya et al. (2013) analyzed the geomechanical consequences using the gas fields (Naylor and Iona) from Australia. Several authors also investigated the surface upliftment at the In Salah CO_2 storage site (Fokker et al., 2011; Newell et al., 2017). However, the simple assumption in the overburden section is used in all the work except Mandal et al. (2021), where they build a gridded overburden static geomechanical model. They used 1D well properties points dataset during interpolating laterally. When limited wells are present, the interpolation method increases the uncertainty significantly. The effect of anisotropic overburden properties in the dynamic simulation is missing in their work. On the contrary, other authors (Olden et al., 2014; Ouellet et al., 2011) did the dynamic simulation but focused on mainly the reservoir and caprock sections and used simple assumptions for the overburden section.

Seismic data have been used for geomechanical models, but only focusing on reservoir and cap rocks sections and not on the whole subsurface (Herwanger and Koutsabeloulis, 2011; Sengupta et al., 2011). The seismic data-driven geomechanical properties of cap and overburden rocks can be a possible solution to fill the data gap because the 3D seismic volume has a full coverage of data from the seafloor to below the reservoir zone. This gap in geomechanical model building motivates us to carry out this research so that we can integrate all the pieces and build a robust geomechanical model to answer the critical questions regarding associated risks during CO_2 injection into the prospective reservoirs. The results from a simple modeling approach might hide possible risks demonstrated in Fig. 1b. Therefore, a high-resolution spatial gridded cap and overburden sections are needed in geomechanical modeling to assess the caprock integrity and realistic overburden rock deformation.This study proposed a workflow to resolve this issue by integrating spatially gridded overburden properties with numerical simulation for stress-strain changes due to CO_2 injection-induced pore pressure change. This research investigates the effect of overburden spatial variability by introducing a seismic properties-based 3D, one-way coupling geomechanical modeling workflow integrating petrophysics, rock physics, and seismic inversion techniques. The main aim is to test the sensitivity of overburden rock properties on rock mechanical failure due to CO_2 injection-related reservoir pressure increase. Moreover, the total vertical displacement of reservoir-caprock interaction is also estimated.

The credibility and practicality of this new modeling approach are

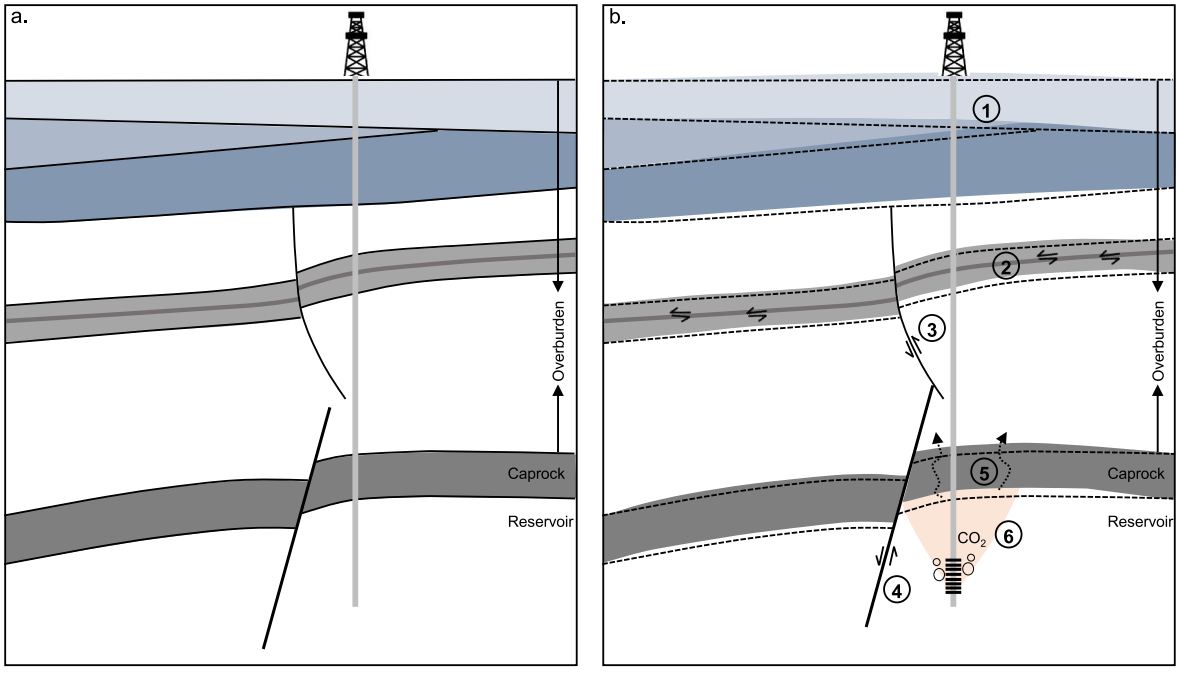

Fig. 1. Schematic representation of CO_2 injection-induced geomechanical effects in a saline storage complex including reservoir, caprock, and overburdens (a) pre-injection state and (b) during/post-injection scenario. Potential consequences include (1) surface heave, (2) bedding parallel slip along with soft layers, (3) & (4) fault reactivation, (5) caprock rock fracturing, and (6) Poro-perm change due to reservoir expansion.

tested using seismic and well log data of the potential CO_2 storage site Smeaheia, offshore Norway. Finally, a field-scale comparative analysis of different models from the Smeaheia injection site is evaluated. To our known reference, the overburden spatial variability on field-scale geomechanical models in CO_2 storage or hydrocarbon production fields is not analyzed before; hence this work is a novel approach in this research arena.

2. Geological setting, cap, and overburden rock properties

The studied Smeaheia area is located in the Horda Platform (HP), northern North Sea, and bounded by two regional N–S trending faults; Vette fault (VF) in the west and Øygarden fault complex (ØFC) in the east (Fig. 2a). The area is positioned east of the giant Troll east gas field and has two structural closures named Alpha (32/4-1) and Beta (32/2-1). Both structures are fault-bounded closures where the Alpha structure is located in the footwall of the Vette Fault, and the Beta structure is located in the hanging wall of the Øygarden Fault Complex (Rahman et al., 2020). These faults are believed to have been formed during the Permo-Triassic 1st rifting event and rooted in the Caledonian zones of crustal weakness (Whipp et al., 2014). During the 1st rifting event, a wide basin with thick syn-depositional wedges is formed in the center of HP, while the 2nd rifting event (Late Jurassic to Mid-Cretaceous times) shifted westward but reactivated all the major faults and formed several smaller faults with minor displacement (Duffy et al., 2015; Skurtveit et al., 2018; Stewart et al., 1995; Whipp et al., 2014). Several small-scale faults/fractures are also created within the overburden section during the post-rift thermal subsidence (Claussen et al., 1999; Mulrooney et al., 2020).

The study area consists of Upper to Middle Jurassic reservoir and caprock pairs where the Sognefjord, Fensfjord, and Krossfjord formation sandstones act as the main reservoir rocks with good to moderate reservoir quality (Dreyer et al., 2005; Fawad et al., 2021a; Holgate et al., 2015) and organic-rich Draupne and Heather formation shales act as the primary seal (Fig. 2b). The reservoir sandstones were deposited in a coastal shallow marine environment and interfingering with Heather Formation. In contrast, the caprock shales (Upper part of the Heather and Draupne Formations) were deposited in an open marine environment with restricted bottom circulation and often anaerobic conditions (NPD, 2021). A thick westward-dipping overburden section (475–800 m) is also present, comprising fine-to coarse-grained siliciclastic packages with occasional carbonate-rich deposits (Faleide et al., 2015).

Overburden rocks play a vital role in vertical surface displacement and sealing effectiveness assessment. Therefore, the overburden rocks properties used in geomechanical modeling work are critical and need to evaluate cautiously. It is crucial to know the complexities of the studied overburden rocks. The complexities varied from basin to basin, but this study tries to assess the effect of simplification of overburden rocks in 3D field-scale geomechanical modeling and the consequences on vertical surface displacement. The overburden rocks in the studied area (i.e., Smeaheia) have complex structural settings. For instance, the Cretaceous and Paleocene rocks are uplifted in the eastern part and eroded by Hordaland unconformity, while thick packages of those units are present in the west (Fig. 3a). Thick Quaternary glacial moraine sediments (Nordland Group) are deposited on top of the Hordaland unconformity. Due to the paleodepositional complexities, lateral depositional and diagenetic variations are observed, leading to various elastic and mechanical properties in the lateral and vertical directions (Fig. 3). Moreover, the inverted seismic cubes showed a good agreement between the rock properties with geophysical data (Fawad et al., 2021a & b).

In geomechanical modeling workflow, constant properties of overburden, sideburden, and underburden geomechanical grids usually added with the spatially gridded reservoir model to mitigate the boundary effects and bending artifacts (Ouellet et al., 2011). However, considering the data range estimated from the seismic inversion (Fawad et al., 2021a & b) in the study area (Table 1), it is evident that a constant value for the whole overburden section might be over-simplification resulting in the omission of the actual mechanical risks. For instance, Young's modulus (E) of overburden rocks ranges between 0.4 and 2.57 GPa with an average value of 1.53 GPa. The difference is considerably large. Other properties also follow a similar trend with a significant difference between the minimum and maximum values. These overburden properties range indicates the urgency to have the spatially distributed overburden grids in 3D geomechanical model risk

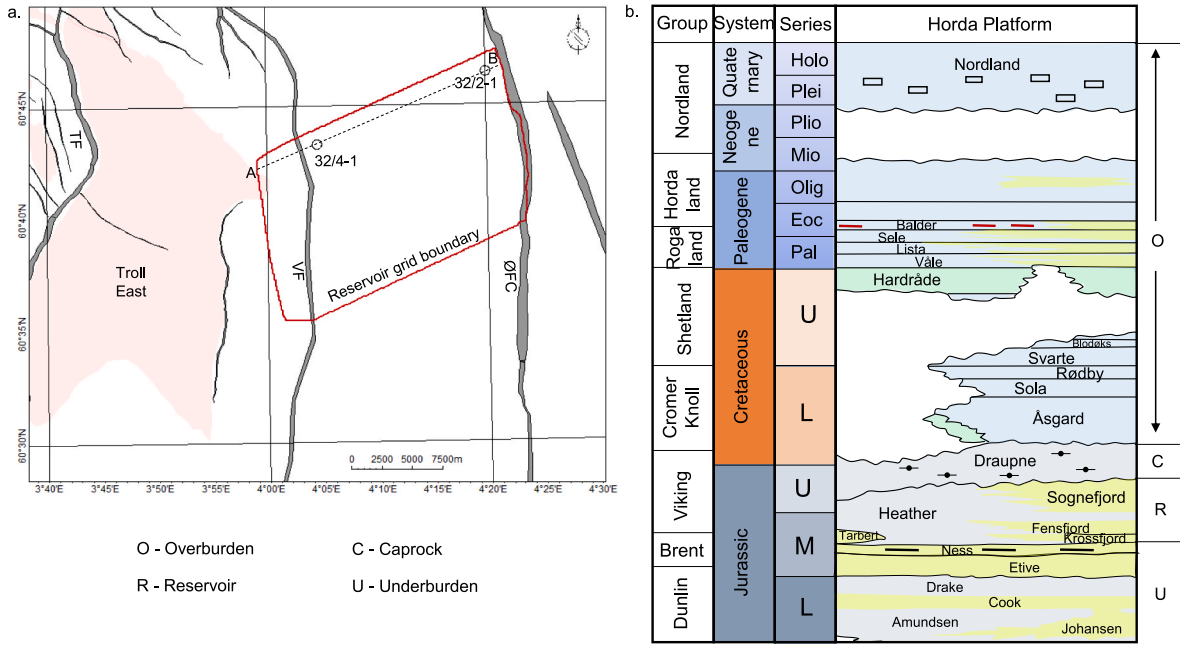

Fig. 2. The red polygon shows the studied model boundary located in the Horda Platform, offshore Norway (a). The area is placed east of the giant Troll east gas field and bounded by two major faults (Vette and Øygarden). The grey shaded lines represent major (*TF – Tusse fault; VF – Vette fault; ØFC – Øygarden fault complex*) and minor faults, and the dotted line indicates the cross-section A to B through the exploration wells 32/4-1 and 32/2-1. This cross-section is used later in the sub-section. (b) A generalized stratigraphic succession of Horda Platform covering the section from Lower Jurassic to the Quaternary (modified after NPD CO_2 Atlas, 2014).

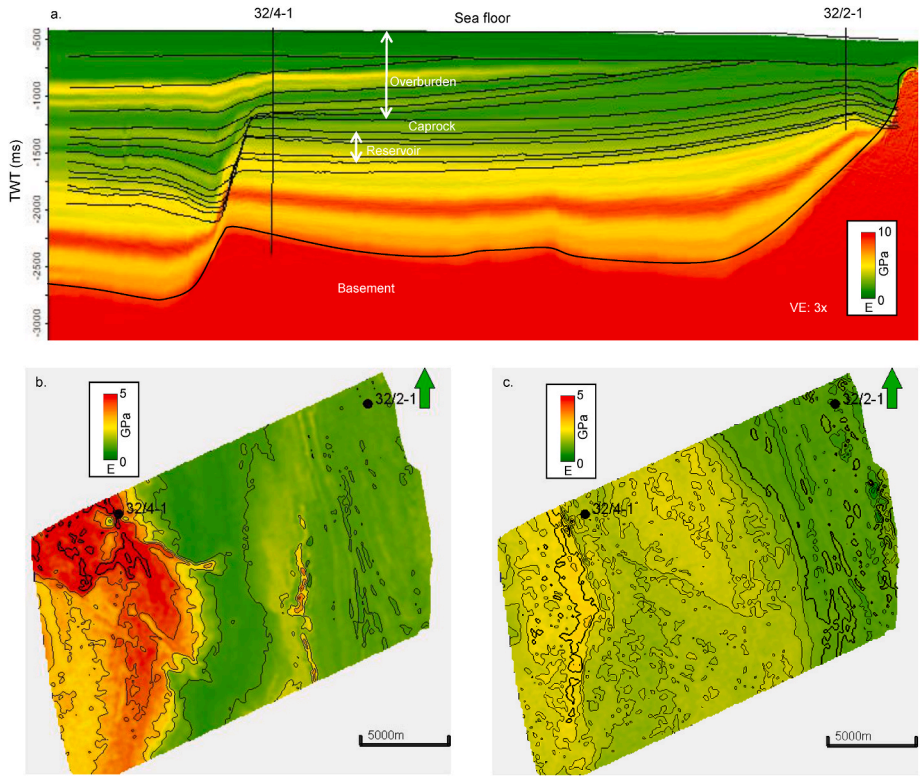

Fig. 3. The spatial and vertical distributions of seismic data-derived Young's modulus (E) shows the W-E cross-section A to B (marked on Fig. 2) view with reservoir, caprock, and overburden horizons and wells (a). The extracted E on top of Lista (b) and Rødby (c) formations demonstrated the lateral variations of rock properties within the overburden.

Table 1
Overburden properties of density, Young's modulus (E), Poisson's ratio (PR), Friction angle (FA), and Unconfined compressional stress (UCS) show the minimum, average and maximum values in the study area.

	Density (gm/cc)	E (GPa)	PR	FA (^{0})	UCS (MPa)
Min	2.14	0.4	0.35	24.51	5.02
Avg	2.24	1.53	0.39	25.92	10.90
Max	2.31	2.57	0.45	26.96	16.46

assessment.

3. Database and workflow

The field-scale reservoir model structural grid is constructed using the seismic interpreted surfaces. The seismic interpretation (i.e., horizons and faults) is carried out using a 3D post-stack seismic volume named GN1101 and two available wells 32/4-1 and 32/2-1 (Fig. 2a). Moreover, pre-stack simultaneous inversion (Fawad et al., 2021a & b) is carried out to invert 3D properties to estimate porosity, Young's Modulus (E), Poisson's Ratio (PR), and Density cubes to populate properties within the structural grids and volume of clay (Vsh), and P-sonic (DT) cubes are used to estimate Friction Angle (FA) and Unconfined Compressional Stress (UCS), respectively.

Fig. 4 illustrates the workflow used in this research to estimate field-scale rocks stress and strain in one-way coupling geomechanical modeling project. The 3D seismic inverted property cubes, which is calibrated with lab measurement and wireline logs during estimation, are directly used in the 3D structural grid. The seismic resampling function in the Petrel-2019 earth modeling module is used to distribute the properties within the model grids. However, the structural grid is constructed earlier, using the seismic interpreted time surfaces. Afterward, the whole reservoir model (i.e., structural grid and properties) is converted into depth using the Smeahiea average velocity cube. Geomechanical grid is introduced in-depth domain by adding sideburden, underburden, overburden, and plate with the reservoir grid. The boundary conditions (i.e., present tectonic stresses and pore pressure) have been defined. The model is now ready for numerical simulation; hence, the VISAGE simulator (Ouellet et al., 2011) is used to run one-way coupling (i.e., changing strain with stress change). After calibration with the observed stresses, the numerically simulated field-scale 3D model is transferred to the Petrel software for interpretation when the estimated value shows a reasonable outcome. This is the workflow we used in this research to run and interpret our models (described in detail later).

4. Model setup

A detailed description of the reservoir and geomechanical modeling structures are described in this section. In each sub-section, the reservoir model describes first, which follows the description of the geomechanical model. Please note that the model time to depth conversion is performed after reservoir model elastic and strength properties distribution.

4.1. Model scenarios

The main focus of this research is to assess the effect of the constant (isotropic) overburden properties versus the spatially distributed true (anisotropic) properties on vertical displacement and changes of strain. Therefore, four models are run to see the overburden sensitivity (Table 2), where model 1 (M-1) has the spatially distributed overburden properties from seismic. In contrast, the rest of the models (M-2, M-3 & M-4) have constant overburden properties with the minimum, mean and maximum values (Table 1), respectively. Please note that the models have the same reservoir and caprock seismic driven properties (Fawad

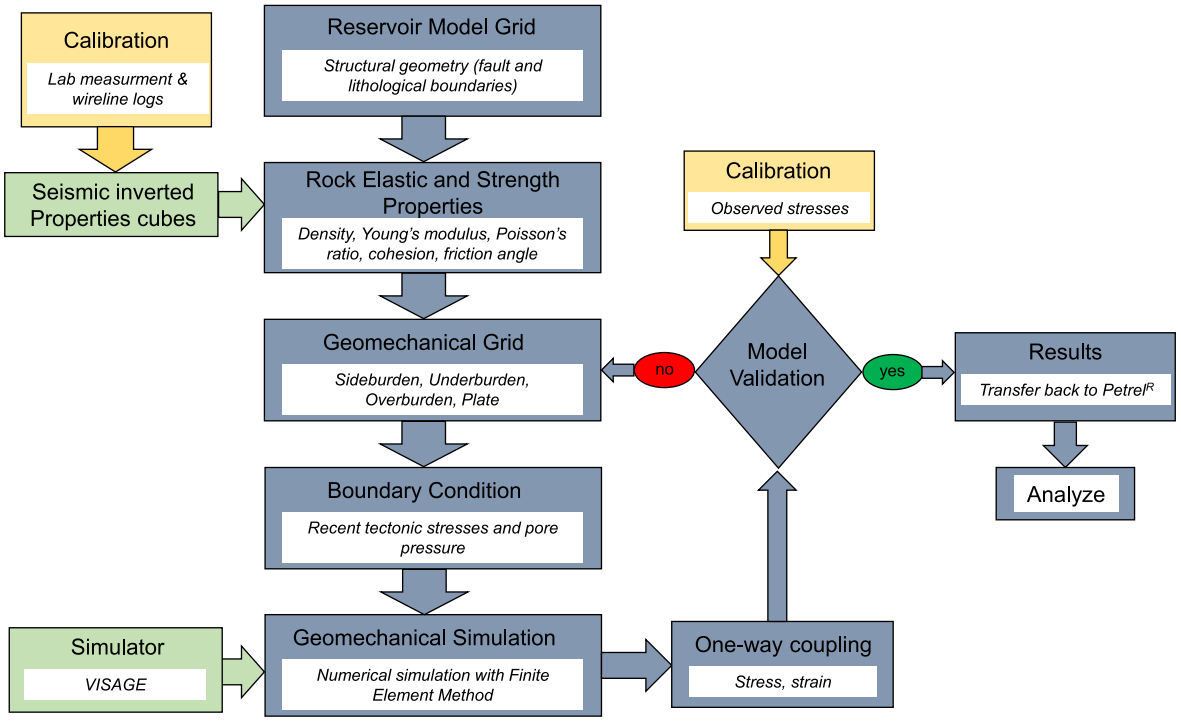

Fig. 4. Seismic properties based one-way coupling field-scale 3D geomechanical modeling workflow used in this research.

Table 2
The criteria used for various models tested in this research.

Model no.	Comments
M-1	Model with overburden reservoir grid and spatially distributed properties
M-2	Model with overburden geomechanical grid and minimal constant properties
M-3	Model with overburden geomechanical grid and average constant properties
M-4	Model with overburden geomechanical grid and maxmimum constant properties

et al., 2021a & b) with the same number of grids.

The reservoir simulation model is out of the scope of this study; hence there is no direct grid by grid pressure increase due to CO_2 injection data being available. Instead, in the one-way coupling, the reservoir simulation result of the Gassnova study is adapted (Gassnova, 2012). However, different model grids require a constant increase in reservoir pressure in different time steps. In the Gassnova model, a total of 160 MT of CO_2 is injected for 50 years with a 3.2 MT/year rate. The average reservoir porosity is 0.26, while the permeability is 690 mD, and the Kv/Kh ratio is equal to 0.1. No solubility of CO_2 into the water function is used because a minor effect has been observed during the sensitivity study (Gassnova, 2012). We assess five (5) different time steps for one-way coupling starting from the initial hydrostatic scenario with every 10-years time step (Fig. 5). Because the main objective of this study is to evaluate the overburden spatial rock sensitivity, we do not consider other time steps such as every 5 years or every year scenario. The hydrostatic initial reservoir pressure is increased constantly throughout the model by multiplying the percentage adapted for each time step from the Gassonova reservoir simulation model. However, in the fluid simulation model, the CO_2 plume will migrate in a specific area and direction based on the poro-perm and structural dip; hence, the reservoir pressure will be varied spatially. Nonetheless, this study has no effect because the same reservoir pressure increase scenarios are used in all the models.

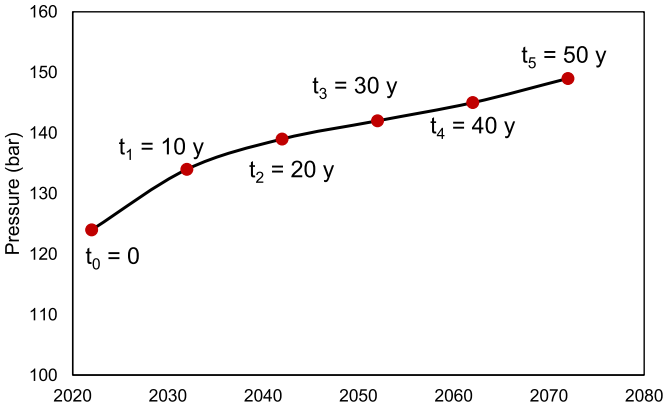

Fig. 5. Reservoir pressures in different time steps adapted from the Gassnova reservoir simulation model (Gassnova, 2012).

4.2. Structural grid

Two sets of reservoir grids are prepared using Petrel structural modeling platform to analyze the overburden rock sensitivity. The first structural grid is for M-1 consists of 14 time surfaces interpreted from the 3D seismic cube (GN1101). This model comprises 13 zones, out of which 7 zones are from the overburden section, and the lowermost zone is underburden rock (Dunlin Group). The total number of vertical layers

Table 3
Statistical comparison of reservoir grids constructed for Model-1 and Models-2/-3/-4.

	Reservoir Grid		Geomechanical Grid	
	M-1	M-2/-3/-4	M-1	M-2/-3/-4
No of horizons	14	6	16	8
No. of zones	13	5	15	7
No. of layers	44	21	48	27
No. of grid cells	340,692	158,928	442,320	243,648

is 44, with more than 340 thousand active grid cells (Table 3). On the contrary, the reservoir grids for M-2/-3/-4 are consist of only caprock and reservoirs with 6 horizons and 5 zones (1 caprock and 4 reservoirs zone). Moreover, the total layers and grid cells are much lower than the first grid with 21 and 158 thousand, respectively. The reservoir grid covers an area of 22 × 13 km^2 (Fig. 5), while each grid covers an area of 250 × 250 m^2. The faults (i.e., Vette, Øygarden, and minor faults) are also considered during seismic horizon interpretation. However, a separate fault grid with different properties is not assigned for model simplicity.

The reservoir grid is expanded laterally and vertically while building the geomechanical grid to mitigate boundary effects and buckling artifacts over the domain of interest. The original reservoir grids with the properties keep unchanged for both grids. The M-1 grid does not need overburden because the overburden section is included within the reservoir grid. Therefore, the sideburden and underburden are added to the reservoir grid for M-1, and sideburden, underburden, and overburden are added to the later grid. Along with the sideburden direction (horizontal), the size of neighboring cells increases by a factor of 1.5 from the edge of the reservoir grid to the edge of the geomechanical grid and covers an area of 68 × 69 km^2 (Fig. 6). The vertical thickness used 5 km; hence the additional depth is adjusted by adding additional underburden in both geomechanical grids.

4.3. Model properties

The seismic inverted rock deformation and rock strength properties are resampling using the geometrical modeling function in Petrel-2019. The interpolate function is used where each cell is a weighted interpolation of 4 seismic cells closest to the center of the grid cell. The prestack seismic inverted property cubes are estimated using an algorithm based on modified Fatti three reflectivity terms (Fatti et al., 1994; Fawad et al., 2020; Hampson et al., 2005). Five partial stacks with angles 0-10^0, 10-20^0, 20-30^0, 30-40^0, and 40-50^0 are used as the input data for the prestack simultaneous inversion (Fawad et al., 2021a). The properties such as porosity, density, Young's modulus (E), Poisson's ratio (PR) are estimated from seismic inversion and directly resampled within the grid, while the other inverted cubes such as volume of shale (Vsh) and P-sonic (DT) are used to calculate friction angle (FA) and unconfined compressive stress (UCS) properties. The FA is estimated using a linear equation based on Vsh and stated that:

$$FA = -12.5Vsh + 32.5 \quad (1)$$

where the sand point (Vsh = 0) and shale point (Vsh = 1), the FA values are used as 32.5 and 20, respectively. The UCS is estimated from P-sonic (DT) using the equation proposed by Horsrud (2001):

$$UCS = 0.77(304.8/DT)^{2.93} \quad (2)$$

where, DT is the P-sonic in μs/ft, and UCS is in MPa.

Fig. 7 illustrates the cross-sectional view (AB marked on Fig. 2) of Young's modulus property distributed within the reservoir grids. The spatially distributed overburden model (M-1) shows property variations within the overburden section (Fig. 7a), while the other model (Fig. 7b) indicated no overburden reservoir grid; hence, no lateral distribution. However, in the geomechanical grid, constant overburden, sideburden,

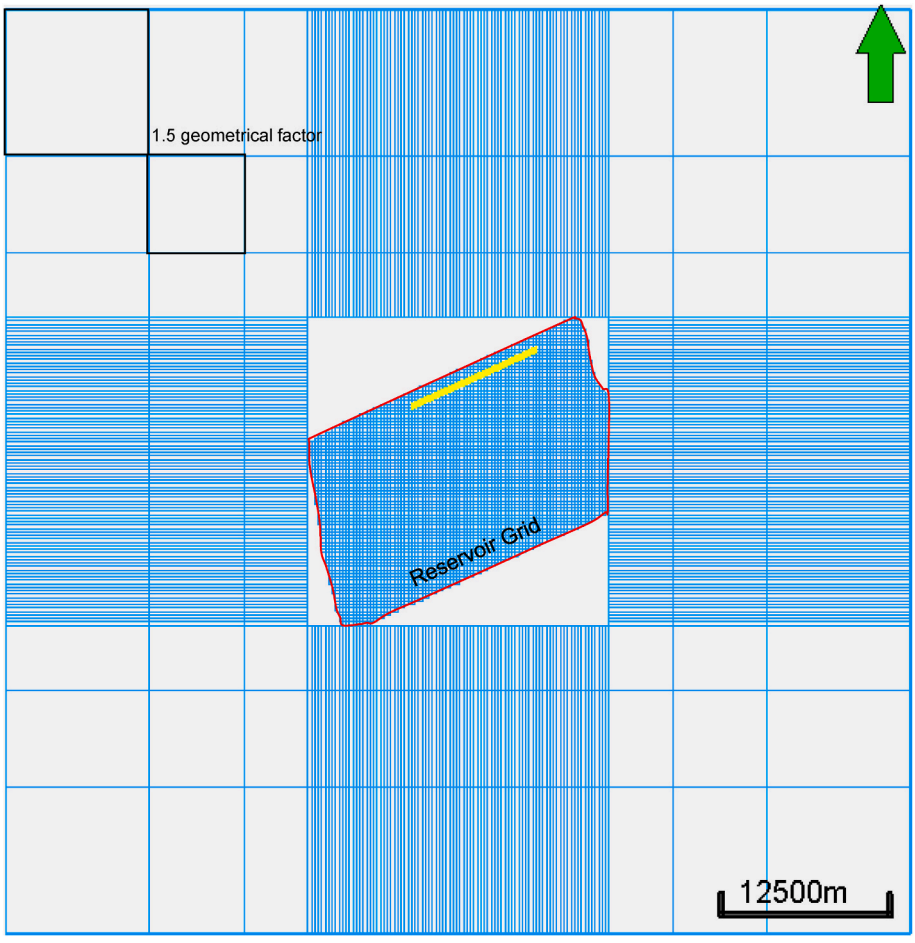

Fig. 6. The model grid shows the reservoir and geomechanical grids distribution. The reservoir grid remains unchanged, while the geomechanical grid used a 1.5 geometrical factor when added.

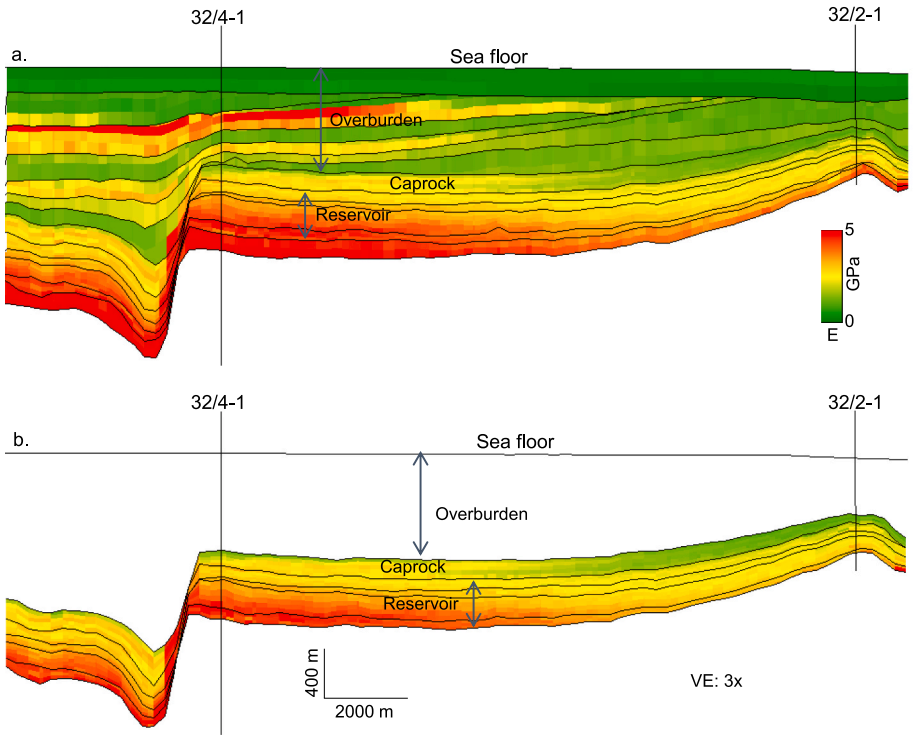

Fig. 7. Cross-section of seismic inverted Young's modulus distributed within the reservoir model grid (a) spatially distributed overburden (M-1) and (b) constant overburden properties (M-2, -3 & −4).

and underburden values are used. Different models are tested using various overburden properties, while the sideburden and underburden properties are the same for all geomechanical grids. Average properties of Dunlin Group are used for underburden, while the caprock properties are used for sideburden grids. A 50 m stiff plate is also added at the edge of the geomechanical grid, which allows us to distribute the pressure within the grids uniformly. In addition, a Mohr-Coulomb failure criteria-based model is assigned. The sensitivity of Biot's coefficient is not tested in this research; instead, it used 1 in all models. Moreover, the thermal effect is out of the scope of this work.

4.4. Pore pressure and in-situ stresses

It is crucial to know the pore pressure to identify the stress field since stress and pore pressure are closely related via poroelastic responses (Grollimund et al., 2001). The large parts of the Norwegian sector show pore pressure close to hydrostatic, including the areas surrounding the Troll and Oseberg fields. Initial hydrostatic reservoir pressure is also applied in this research. Although there is a possibility of depletion due to Troll production, this is not considered in this work.

The in-situ principal stresses in an area depend on many factors and change with time. Moreover, in the study area, very few measurements are available. Based on the present-day seismicity (C-quality data) and leak of test (LOT) data observation, a normal faulting stress regime is assigned in the study area where the vertical stress (lithostatic stress) is the highest principal stress and the minimum horizontal stress is the lowest one (Heidbach et al., 2018; Rahman et al., 2021; Skurtveit et al., 2018). The minimum horizontal stress (SHmin) gradient is used as 0.01245 MPa/m estimated using X-LOT (Rahman et al., 2021), while the maximum horizontal stress (SHmax) assumed 10% more stress than SHmin (Fig. 8). Moreover, based on the seismicity database near Troll field, SHmax azimuthal direction is used as 103^0 (Heidbach et al., 2018).

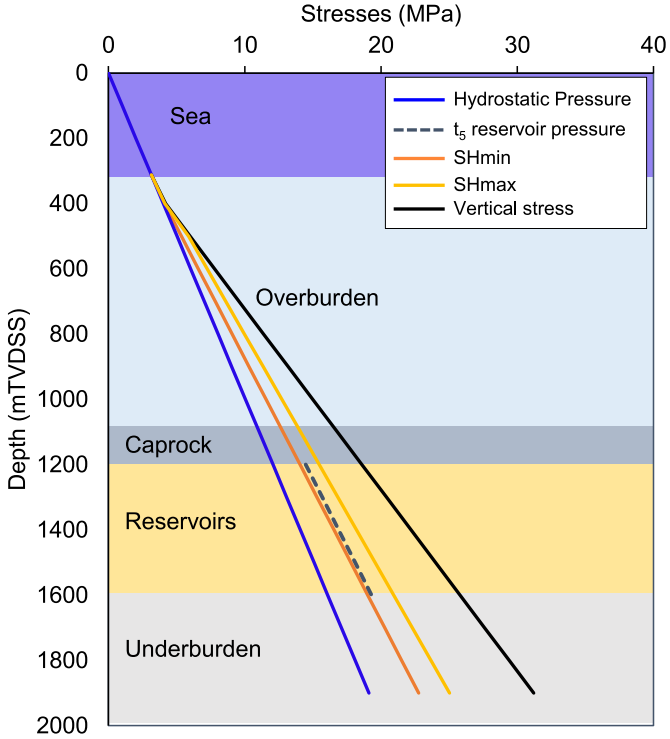

Fig. 8. The pore pressure and in-situ stresses in Alpha well (32/4-1) location assuming a normal faulting regime (modified after Rahman et al., 2021). The reservoir pressure increase after 50 years of injection (t_5) is also illustrated for reference.

4.5. Simulator

In this study, the VISAGE finite element mechanical simulator has been used to conduct one-way coupling (Ouellet et al., 2011). The static model preparation and simulation cases are defined in the Petrel-2019 platform. When the model cases are ready, a VISAGE plug-in is used to iterate the defined models. As we used plug-in, the model results are directly available in the Petrel platform to analyze.

5. Results

The one-way coupling simulation is conducted using 5 different reservoir pressure scenarios illustrated in Fig. 9. The t_0 time represents the initial hydrostatic reservoir pressure which increases with time due to CO_2 injection in every 10-years time step. It is worth mentioning that the pressure increment is only applied within the Vette- Øygarden fault block (Fig. 9). Each pressure grid is assigned a time step mentioned in Fig. 5. As expected, the pressure increases from initial (t_0) to t_1 is significant. After that, the increment is more gentle but has slight lateral variation.

5.1. Ground deformation (seafloor)

The estimation of vertical displacement of the seafloor is crucial to assess the suitability of the CO_2 injection sites. The top view of seafloor deformation due to CO_2 injection in various time steps in M-1 is illustrated in Fig. 10. The grid located west of the Vette fault is excluded because no pressure difference is addressed in this section, hence no deformations. The seafloor experienced a gradual uplift with time; however, spatial variation is also observed. Although the trend of lateral dissimilarity for each step shows similarity, it does not follow the pressure increase trends. Moreover, the maximum uplift estimated in M-1 is 7 cm, located in the middle and southern part of the model.

5.2. Vertical displacement on the reservoir-caprock interface

The base layer of the caprock is also assessed to evaluate the deformation in the reservoir-caprock interface (Fig. 11). The grids west of the Vette fault are also excluded from the map-viewed results. Overall, the caprock is uplifted due to CO_2 injection-related reservoir pressure change. The rock deformation gradually increases with time and reaches maximum uplift of 8 cm (at time t_5). However, the increment of rock deformation followed a patchy trend nucleus at the middle-west part of the VF and continued eastward. Moreover, the deformation is observed minimal in both well locations.

5.3. Comparative analysis

One of the main objective of this research is to evaluate the sensitivity of the overburden rock properties. In this section, we assessed that by comparing the models. In addition, the rock deformation difference between seafloor and base caprock is also evaluated.

5.3.1. M-1 versus M-3

The main difference between M-1 and M-3 models is the value of overburden properties and the distribution within grids. In M-1 seismic driven properties are spatially distributed while M-3 represents average constant properties for the whole overburden section. These variations not only significantly influence the seafloor deformations but also affect caprocks. The rock layer's upliftment doubled while using the average constant value compared with actual spatially distributed seismic driven properties. The maximum seafloor upliftment estimated is 7 cm in M-1, while M-3 assessed 14 cm (Fig. 12). A similar trend is also observed in caprock deformation scenarios (i.e., 8 cm and 15 cm in M-1 and M-3, respectively). However, both models (M-1 & M-3) show smooth deformation in seafloor and a patchy upliftment in the base caprock layer. Moreover, base caprock deformed slightly higher compared to the

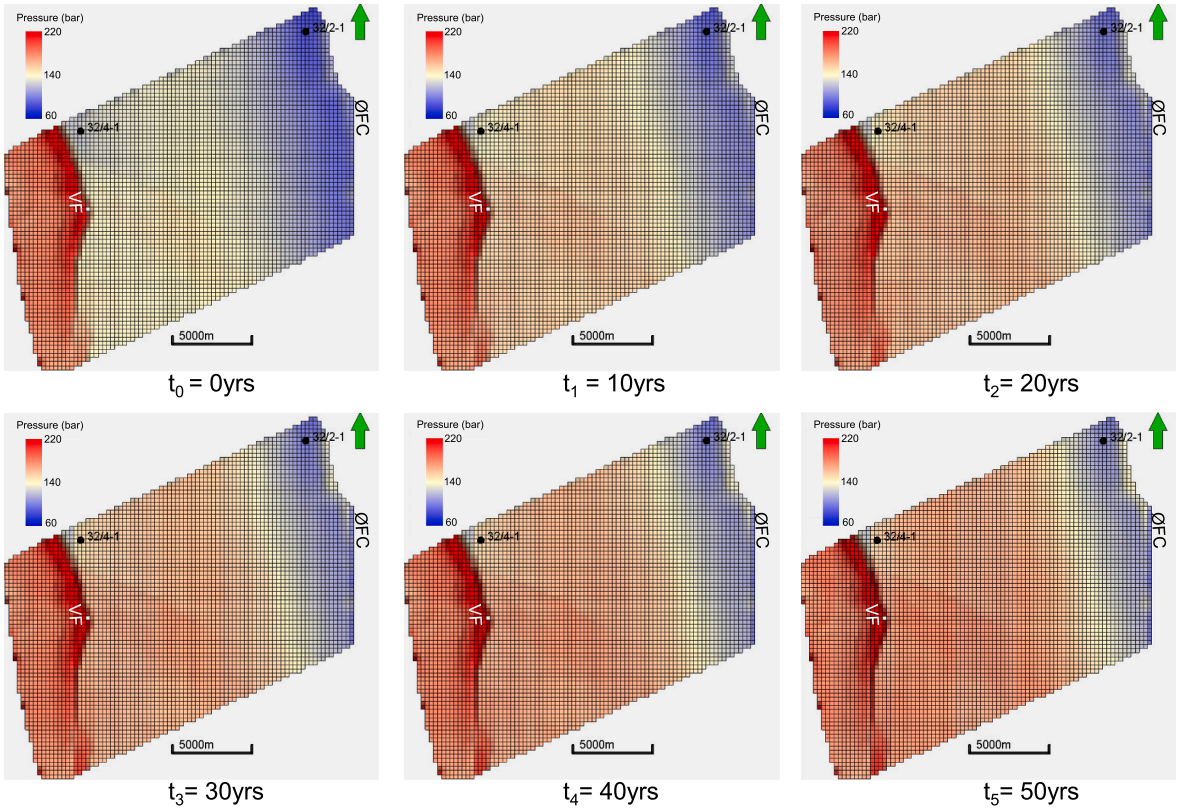

Fig. 9. The top reservoir layer shows the reservoir pressure changes in different time steps. Reservoir pressure increase confined between Øygarden Fault Complex (ØFC) and Vette Fault (VF). Note that there are no pressure changes west of VF.

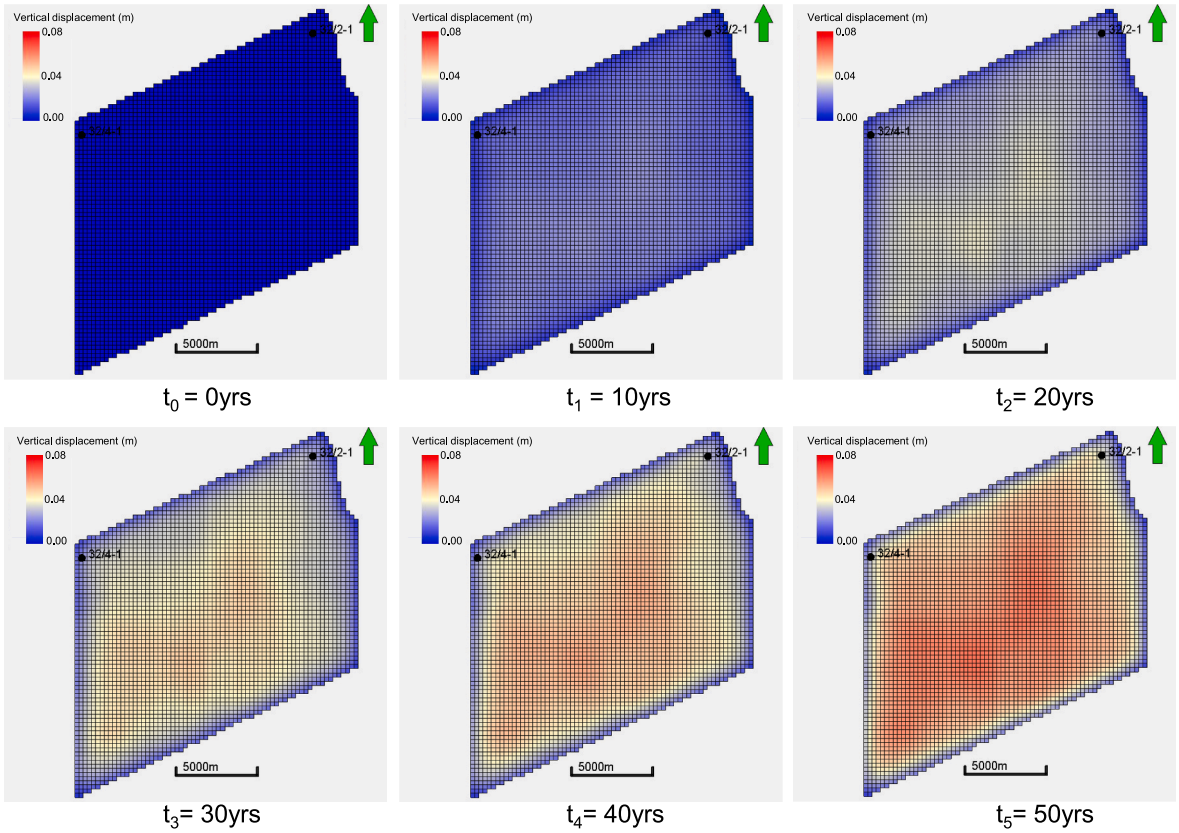

Fig. 10. Vertical displacement in various time steps is estimated in M-1. Seafloor gradually uplifted due to CO_2 injection-related reservoir pressure increase.

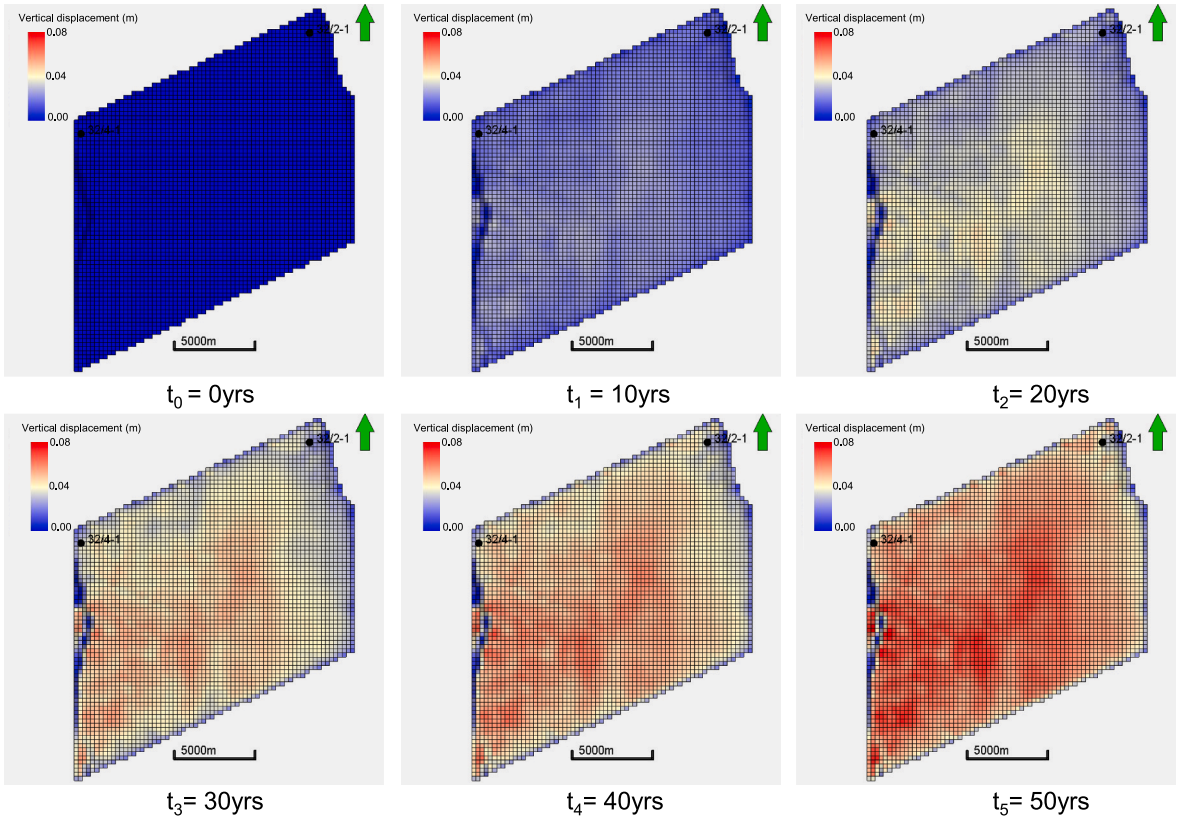

Fig. 11. Estimated vertical displacement of the base layer of caprock in various time steps in M-1. Significant upliftment (~8 cm) is observed just above the reservoir zone.

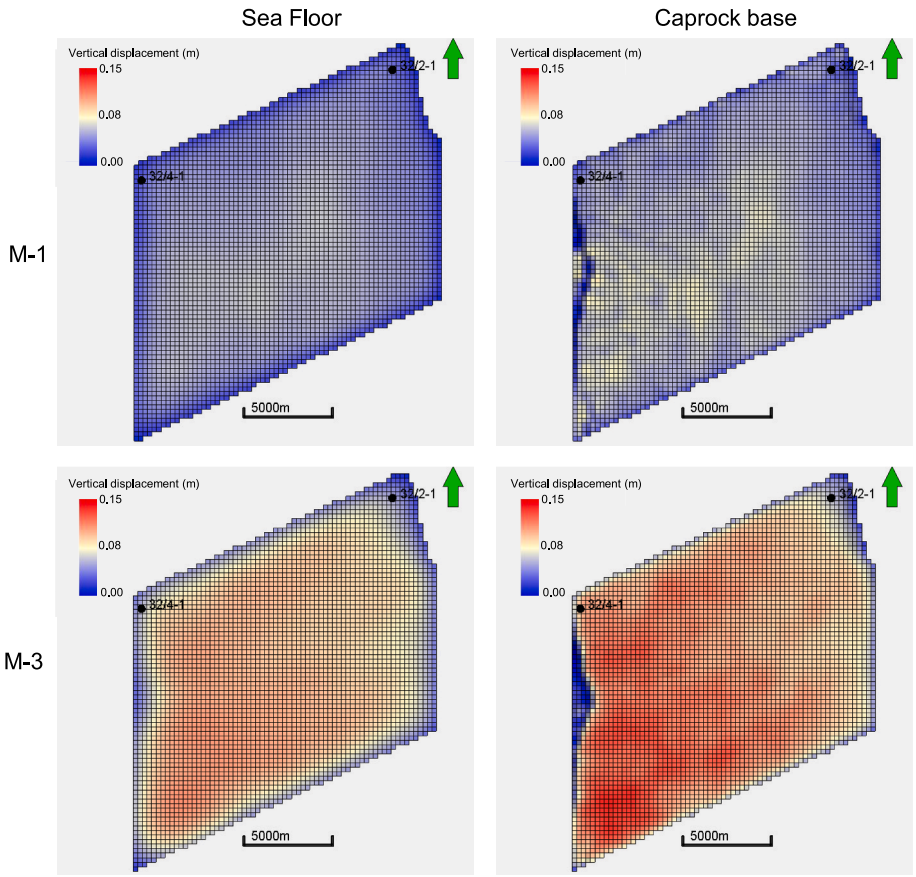

Fig. 12. Vertical displacement of the seafloor and base caprock layers at t_5 time step shows the comparison between M-1 and M-3.

seafloor upliftment.

Similar spatial differences are also observed in the 3-dimensional cross-section of the model M-1 and M-3 (Fig. 13). The cross-section plane shown is in the middle of the model, where the wells (i.e., 32/4-1 and 31/2-1) are displayed for reference. The overburden structural variations are clearly visible, where M-1 followed the actual structural setup (3D seismic interpreted), and in M-3 overburden section is divided into three horizontal layers. The average overburden property model (M-3) significantly changes the vertical upliftment within caprock and overburden sections and influences the upper part of the reservoir (Fig. 13b).

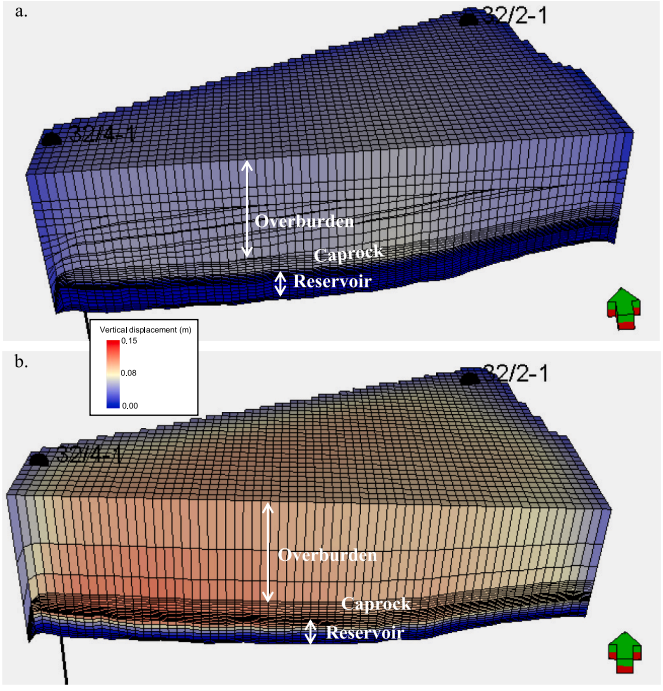

Fig. 13. The difference of vertical displacement between M-1 (a) and M-3 (b) are illustrated three-dimensionally. M-3 model shows significantly higher upliftment compared to M-1.

The differences between M-1 and M-3 are also observed in Mohr-Coulomb failure envelopes. The failure diagrams illustrated in Fig. 14 are located in the middle of the studied grid (i:j; 50:53) where overburden (Fig. 14a&b), caprock (Fig. 14c&d), and reservoir rocks (Fig. 14e and f) are compared. All the stress circles are at the compressive side and below the failure envelope except the M-3 reservoir zone, which indicated that the rock is in shear form with less possibility of matrix deformation. However, in all the scenarios, the chance of shear failure is higher in M-3 compared to M-1. The stress circles are moved to the left due to CO_2 injection within the reservoir. However, in model 3, the t_5 scenario touches the rock compressive strength, which is usually equal to the mean value of maximum principal stress (Ahmed and Al-Jawad, 2020).

5.3.2. *M-2 versus M-3 versus M-4*

Although there is a significant difference observed between M-1 and M-3, the effect of different overburden constant values (Table 2) on 3D model simulation is trivial. The difference between the models in time steps t_1 and t_5 is illustrated in Fig. 15. Due to CO2 injection, the reservoir pressure increases, resulting in a seafloor heave, but that is insignificant. Moreover, the surface deformation trends in all models are similar.

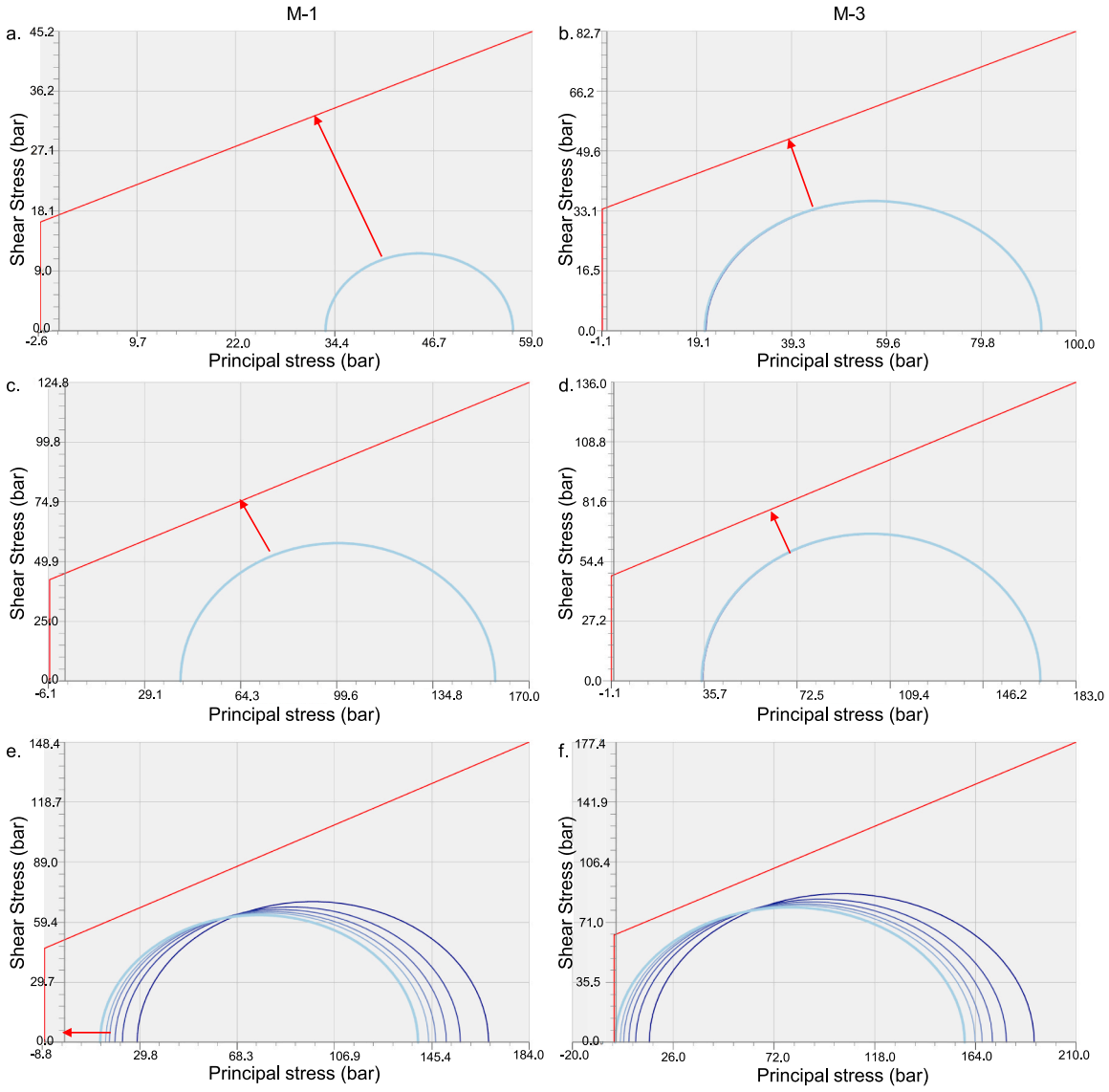

Fig. 14. Mohr-Coulomb diagram of location in the middle of the model (I,j; 50, 53) shows the comparison between the model M-1 and M-3 within overburden (a, b), caprock (c, d), and reservoir (e, f) zones. M-3 represents significantly higher chances of failure compared to M-1. Also, note that both horizontal and vertical scales have differences.

6. Discussion

The geomechanical modeling approach applied in this study shows the practicality. Although the spatially variable overburden properties gridded model (M-1) has a higher number of active cells, the computational time required is not abnormally high (qualitatively, the model required 4 times higher time than the constant properties models). This research also reveals that the seismic inverted properties can be improved to the traditional modeling approach where well data properties are interpolated using different algorithms. Moreover, where the well database is limited, the range of uncertainties are significantly high in 3D space. In this scenario, a seismic-driven approach could be a solution introduced in this study. However, for seismic driven properties modeling workflow explained in this research is dependent on the availability of 3D seismic cube. Moreover, 3D field-scale geomechanical modeling is critical to evaluate injection-related induced mechanical risks in any injection site. Furthermore, this approach allows us to incorporate the complex structural setup.

The fluid simulated reservoir pressure used in this study has a total pore volume model. The base case Gassnova (2012) model included the whole Vette-Øygarden fault block, while the model used in this study covers one-fourth of surface area compared with the Gassnova model. However, the injected reservoir rocks layers are the same; hence, assumed to have similar reservoir quality (i.e., Poro-perm). Although the model area is significantly small in this study, there is no effect on this study's main purpose (i.e., overburden sensitivity). This also indicates the urgency of having a coupled fluid flow – mechanical modeling approach, where we have full control and the ability to evaluate the stress-dependent poro-perm changes.

6.1. *Effect of overburden properties on rock deformation*

Constant overburden model properties might introduce misinterpretation in rock deformation, which leads to poor decisions during site specification. Different overburden rock units have a significant variation in mechanical properties (Fig. 7). A significant difference in vertical rock deformation is also observed (Figs. 12–14). The stress differences between the overburden formations in M-1 have also illustrated the effect of initial mechanical rock properties. Fig. 16 represents the variation of the Mohr-Coulomb failure envelope between different layers

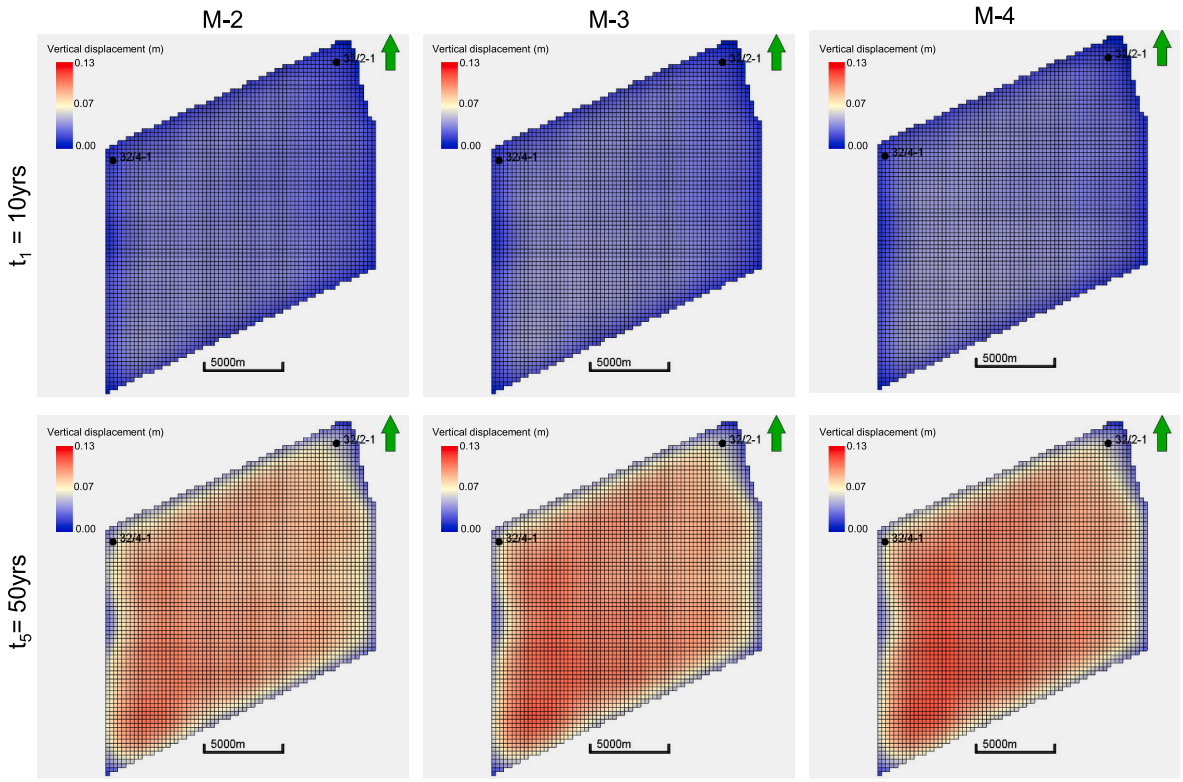

Fig. 15. Seafloor heave in t_1 and t_5 time steps shows the comparison between minimum, average, and maximum constant overburden properties.

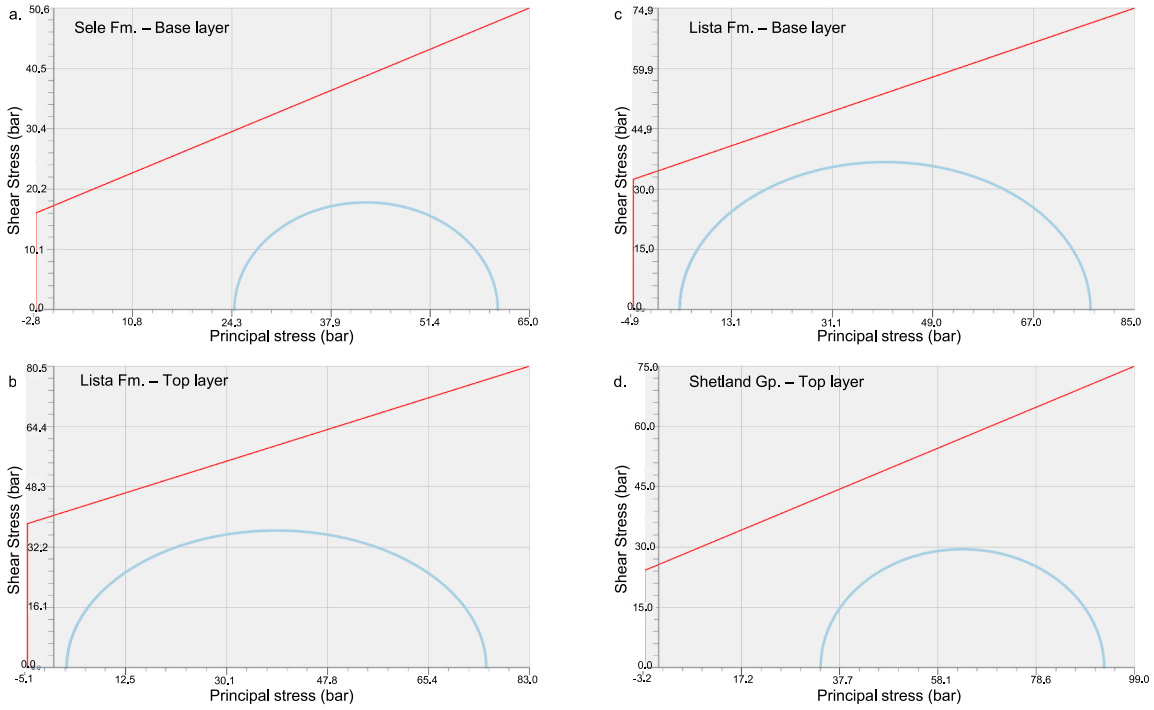

Fig. 16. The variation of failure mode within overburden rocks in M-1 illustrated the Mohr-Coulomb plot of the base layer of Sele Formation (a), the top layer of Lista Formation. (b), base Lista Formation. (c) and top Shetland Group. (d). Please note that both horizontal and vertical scales have differences.

while horizontal location (i & j) remains the same (50 & 53). The Lista Formation shows significantly higher failure possibility (both shear and tensile) compared to the above Sele Formation and below Shetland Group layers. This indicates the importance of using the right overburden properties in geomechanical modeling work. Simplication of model properties might be an over-or underestimation of the rock failure, which leads to a significant issue during real injection scenarios.

6.2. Implication in CCS

The rock deformation due to reservoir pressure change is critical in the subsurface CO_2 storage project. The quantitative assessment of vertical displacement of rocks reveals the failure potential of the cap and overburden rock which determined the seal effectiveness in any injection site. In addition, the mechanical failure threshold of caprock and overburden makes the site non-reliable because of caprock and fault failure. Therefore, vertical rock displacement plays a vital role in decision-making for any injection site evaluation.

The significant influence of caprock properties on rock displacement becomes crucial because the traditional way of including simplified overburden properties in the geomechanical model might lead to inaccurate estimation of the potential of storage and injectivity of any site. The estimate of optimal capacity and injectivity before any failure of any CO_2 injection site is crucial because it defines the safe storage potential of that site. However, to evaluate the total safe storage reservoir capacity, a fluid simulation model needs to couple with the geomechanical model called a two-way coupling model. This study, however, assessed only the stress-strain geomechanical deformations in a specific injection rate and injection time. Although this study cannot estimate the total safe storage capacity and injectivity based on the analysis, the comparative investigation suggested a significant overestimation of potential geomechanical risks might be estimated based on the traditional simple overburden properties model. In this way, we might lose half of our safe storage capacity, which might influence the project decision considerably.

Moreover, this approximate estimation might influence the management to declare the injection site non-economical. Additionally, seafloor installation (i.e., wellhead) might be at risk due to overestimation of seafloor heave, resulting in a possible instability risk that might influence the site-specific decision-making. Although we did not perform the maximum displacement analysis, our rock can hold before failure in this study, 100% increase in seafloor upliftment in M-3 indicated the importance of adding spatially distributed overburden properties in the geomechanical modeling (M-1) approach. However, despite the importance of overburden uncertainties in decision-making, the attempt to quantify overburden uncertainties in decision-making has been discounted in CCS management, especially for geomechanics consideration.

7. Conclusions

The seismic data-driven 3D field-scale geomechanical model workflow shows the value while evaluating the mechanical risks in any CO_2 injection sites. This study proved the efficiency and practicality of such a model. The key findings are as follows:

- The effect of overburden properties on rock deformation is significant. For instance, the simplified average constant overburden properties doubled the seafloor uplift compared to the model using the seismic inverted spatially variable properties. Moreover, the Mohr-Coulomb failure envelopes of overburden rocks indicated the importance of spatial overburden properties within the geomechanical modeling workflow.
- Vertical rock deformation increases with time in both seafloor and interface between the reservoir and caprock. However, the vertical uplift is slightly higher in the reservoir-caprock interface compared to the seafloor.
- Although the induced pressure increase in each time steps used a constant change, the rock deformation spatially varied due to the variation in mechanical properties.
- The simplified assumption of overburden properties in the geomechanical model effect the CO_2 storage project significantly by influencing the capacity and injectivity of any site.

The field-scale 3D geomechanical model workflow proposed in this study is effective and time-efficient to simulate the one-way coupling. However, a two-way coupling with reservoir simulation will reveal the pore volume changes within the reservoir. Therefore, two-way partial or fully coupling methods will be the future study.

Credit author statement

Md Jamilur Rahman: Conceptualization, Methodology, Formal analysis, Investigation, Writing – original draft, Writing – review & editing, Visualization, Software. Manzar Fawad: Writing – review & editing, Supervision. Jung Chan Choi: Writing – review & editing, Supervision. Nazmul Haque Mondol: Writing – review & editing, Supervision, Project administration, Funding acquisition

Declaration of competing interest

The authors declare that they have no known competing financial interests or personal relationships that could have appeared to influence the work reported in this paper.

Acknowledgments

We are grateful for the financial support provided by the Research Council of Norway for the OASIS (Overburden Analysis and Seal Integrity Study for CO_2 Sequestration in the North Sea) project (NFR-CLIMIT project #280472). We are indebted to the additional funding and data provided by Norwegian Petroleum Directorate (NPD), Gassnova, Equinor, and TotalEnergies. Thank you very much for the academic software licenses provided by Schlumberger for Petrel-2019 and the VISAGE simulator.

References

Addis, M.A., 1997. The stress-depletion response of reservoirs. In: SPE Annual Technical Conference and Exhibition. Society of Petroleum Engineers.

Ahmed, B.I., Al-Jawad, M.S., 2020. Geomechanical modelling and two-way coupling simulation for carbonate gas reservoir. J. Pet. Explor. Prod. Technol. 10, 3619–3648.

Chiaramonte, L., White, J.A., Trainor-Guitton, W., 2015. Probabilistic geomechanical analysis of compartmentalization at the Snøhvit CO2 sequestration project. J. Geophys. Res. Solid Earth 120, 1195–1209.

Clausen, J.A., Gabrielsen, R.H., Reksnes, P.A., Nysaether, E., 1999. Development of intraformational (Oligocene-Miocene) faults in the northern North Sea: influence of remote stresses and doming of Fennoscandia. J. Struct. Geol. 21, 1457–1475. https://nam11.safelinks.protection.outlook.com/?url=https%3A%2F%2Fdoi.org%2F10.1016%2FS0191-8141&data=04%7C01%7Cs.venkiteswaran%40elsevier.com%7Cdf73c34b4fd046b2a0c708d9ed509086%7C9274ee3f94254109a27f9fb15c10675d%7C0%7C0%7C637801753841890024%7CUnknown%7CTWFpbGZsb3d8eyJWIjoiMC4wLjAwMDAiLCJQIjoiV2luMzIiLCJBTiI6Ik1haWwiLCJXVCI6Mn0%3D%7C1000&sdata=oagJ1Lmjhs%2FERdAowDUZ2aFm9BaSWMdUXucem6NBI6c%3D&reserved=0(99)00083-8.

Dreyer, T., Whitaker, M., Dexter, J., Flesche, H., Larsen, E., 2005. From spit system to tide-dominated delta: integrated reservoir model of the Upper Jurassic Sognefjord Formation on the Troll West Field. In: Geological Society, London, Petroleum Geology Conference Series. Geological Society of London, pp. 423–448.

Duffy, O.B., Bell, R.E., Jackson, C.A.-L., Gawthorpe, R.L., Whipp, P.S., 2015. Fault growth and interactions in a multiphase rift fault network: Horda Platform, Norwegian North Sea. J. Struct. Geol. 80, 99–119.

Faleide, J.I., Bjørlykke, K., Gabrielsen, R.H., 2015. Geology of the Norwegian continental Shelf. In: Petroleum Geosciences: from Sedimentary Environments to Rock Physics, pp. 603–637.

Fatti, J.L., Smith, G.C., Vail, P.J., Strauss, P.J., Levitt, P.R., 1994. Detection of gas in sandstone reservoirs using AVO analysis: a 3-D seismic case history using the Geostack technique. Geophysics 59, 1362–1376.

Fawad, M., Hansen, J.A., Mondol, N.H., 2020. Seismic-fluid detection-a review. Earth Sci. Rev., 103347

Fawad, M., Rahman, M.J., Mondol, N.H., 2021a. Seismic reservoir characterization of potential CO2 storage reservoir sandstones in Smeaheia area, Northern North Sea. J. Petrol. Sci. Eng. 205, 108812.

Fawad, M., Rahman, M.J., Mondol, N.H., 2021b. Seismic-derived geomechanical properties of potential CO2 storage reservoir and cap rock in Smeaheia area, northern North Sea. Lead. Edge 40, 254–260.

Fischer, K., Henk, A., 2013. A workflow for building and calibrating 3-D geomechanical models &ndash a case study for a gas reservoir in the North German Basin. Solid Earth 4, 347–355.

Fokker, P.A., Orlic, B., Van der Meer, L.G.H., Geel, C.R., 2011. Geomechanical modeling of surface uplift around well KB-502 at the in Salah CO2 storage site. In: 73rd EAGE Conference and Exhibition Incorporating SPE EUROPEC 2011. European Association of Geoscientists & Engineers p. cp-238.

Gassnova, 2012. Troll Kystnær Subsurface Status Report.

Grasso, J.-R., 1992. Mechanics of seismic instabilities induced by the recovery of hydrocarbons. Pure Appl. Geophys. 139, 507–534.

Grollimund, B., Zoback, M.D., 2003. Impact of glacially induced stress changes on fault-seal integrity offshore Norway. Am. Assoc. Petrol. Geol. Bull. 87, 493–506.

Grollimund, B., Zoback, M.D., Wiprut, D.J., Arnesen, L., 2001. Stress orientation, pore pressure and least principal stress in the Norwegian sector of the North Sea. Petrol. Geosci. 7, 173–180.

Hampson, D.P., Russell, B.H., Bankhead, B., 2005. Simultaneous inversion of pre-stack seismic data. In: SEG Technical Program Expanded Abstracts 2005. Society of Exploration Geophysicists, pp. 1633–1637.

Hawkes, C.D., McLellan, P.J., Bachu, S., 2005. Geomechanical factors affecting geological storage of CO2 in depleted oil and gas reservoirs. J. Can. Pet. Technol. 44.

Heidbach, O., Rajabi, M., Cui, X., Fuchs, K., Müller, B., Reinecker, J., Reiter, K., Tingay, M., Wenzel, F., Xie, F., 2018. The World Stress Map database release 2016: crustal stress pattern across scales. Tectonophysics 744, 484–498.

Herwanger, J., Koutsabeloulis, N., 2011. Seismic Geomechanics. How to Build Calibrate Geomech. Model. Using 3D 4D Seism. Data EAGE Publ.

Hillis, R.R., 2001. Coupled changes in pore pressure and stress in oil fields and sedimentary basins. Petrol. Geosci. 7, 419–425.

Holgate, N.E., Jackson, C.A.L., Hampson, G.J., Dreyer, T., 2015. Seismic stratigraphic analysis of the middle jurassic Krossfjord and Fensfjord formations, Troll oil and gas field, northern North Sea. Mar. Petrol. Geol. 68, 352–380.

Horsrud, P., 2001. Estimating mechanical properties of shale from empirical correlations. SPE Drill. Complet. 16, 68–73.

Ingram, G.M., Urai, J.L., Naylor, M.A., 1997. Sealing processes and top seal assessment. In: Norwegian Petroleum Society Special Publications. Elsevier, pp. 165–174.

Mandal, P.P., Essa, I., Saha, S., Rezaee, R., 2021. Multi-purpose Utility of Constructing 3D Static Geomechanical Model in the Ichthys Field, Browse Basin. 3rd AEGC Geosci. Sustain. World.

Mulrooney, M.J., Osmond, J.L., Skurtveit, E., Faleide, J.I., Braathen, A., 2020. Structural analysis of the Smeaheia fault block, a potential CO2 storage site, northern Horda Platform, North Sea. Mar. Pet. Geol. 121, 104598. https://nam11.safelinks.protection.outlook.com/?url=https%3A%2F%2Fdoi.org%2F10.1016%2Fj.marpetgeo.2020.104598&data=04%7C01%7Cs.venkiteswaran%40elsevier.com%7Cdf73c34b4fd046b2a0c708d9ed509086%7C9274ee3f94254109a27f9fb15c10675d%7C0%7C0%7C637801753841890024%7CUnknown%7CTWFpbGZsb3d8eyJWIjoiMC4wLjAwMDAiLCJQIjoiV2luMzIiLCJBTiI6Ik1haWwiLCJXVCI6Mn0%3D%7C1000&sdata=29BBiTDlAheqJEq%2BQtAKR%2BfSxe8OdpCcRlaVi%2Fefar0%3D&reserved=0.

Newell, P., Yoon, H., Martinez, M.J., Bishop, J.E., Bryant, S.L., 2017. Investigation of the influence of geomechanical and hydrogeological properties on surface uplift at in Salah. J. Petrol. Sci. Eng. 155, 34–45.

Northern Lights https://northernlightsccs.com/what-we-do/.

NPD, 2021. NPD FactPages [WWW Document]. URL. https://npdfactpages.npd.no/factpages/Default.aspx?culture=en.

NPD CO2 Atlas, 2014. Report.

Olden, P., Jin, M., Pickup, G., Mackay, E., Hamilton, S., Somerville, J., Todd, A., 2014. Geomechanical modelling of CO2 geological storage with the use of site specific rock mechanics laboratory data. Petrol. Geosci. 20, 323–337.

Ouellet, A., Bérard, T., Desroches, J., Frykman, P., Welsh, P., Minton, J., Pamukcu, Y., Hurter, S., Schmidt-Hattenberger, C., 2011. Reservoir geomechanics for assessing containment in CO2 storage: a case study at Ketzin, Germany. Energy Proc. 4, 3298–3305.

Park, J.-W., Guglielmi, Y., Graupner, B., Rutqvist, J., Kim, T., Park, E.-S., Lee, C., 2020. Modeling of fluid injection-induced fault reactivation using coupled fluid flow and mechanical interface model. Int. J. Rock Mech. Min. Sci. 132, 104373.

Rahman, M.J., Choi, J.C., Fawad, M., Mondol, N.H., 2021. Probabilistic analysis of Vette fault stability in potential CO2 storage site Smeaheia, offshore Norway. Int. J. Greenh. Gas Control 108, 103315. https://doi.org/10.1016/j.ijggc.2021.103315.

Rahman, M.J., Fawad, M., Mondol, N.H., 2020. Organic-rich shale caprock properties of potential CO2 storage sites in the northern North Sea, offshore Norway. Mar. Petrol. Geol. 122, 104665.

Rutqvist, J., Birkholzer, J., Cappa, F., Tsang, C.-F., 2007. Estimating maximum sustainable injection pressure during geological sequestration of CO2 using coupled fluid flow and geomechanical fault-slip analysis. Energy Convers. Manag. 48, 1798–1807.

Rutqvist, J., Birkholzer, J.T., Tsang, C.-F., 2008. Coupled reservoir–geomechanical analysis of the potential for tensile and shear failure associated with CO2 injection in multilayered reservoir–caprock systems. Int. J. Rock Mech. Min. Sci. 45, 132–143.

Segall, P., 1989. Earthquakes triggered by fluid extraction. Geology 17, 942–946.

Sengupta, M., Dai, J., Volterrani, S., Dutta, N., Rao, N.S., Al-Qadeeri, B., Kidambi, V.K., 2011. Building a seismic-driven 3D geomechanical model in a deep carbonate reservoir. In: SEG Technical Program Expanded Abstracts 2011. Society of Exploration Geophysicists, pp. 2069–2073.

Skurtveit, E., Choi, J.C., Osmond, J., Mulrooney, M., Braathen, A., 2018. 3D fault integrity screening for smeaheia CO2 injection site. In: 14th Greenhouse Gas Control Technologies Conference Melbourne, pp. 21–26.

Soltanzadeh, H., Hawkes, C.D., 2008. Semi-analytical models for stress change and fault reactivation induced by reservoir production and injection. J. Petrol. Sci. Eng. 60, 71–85.

Stewart, D.J., Schwander, M., Bolle, L., 1995. Jurassic depositional systems of the Horda Platform, Norwegian North Sea: practical consequences of applying sequence stratigraphic models. Nor. Pet. Soc. Spec. Publ. 291–323.

Streit, J.E., Hillis, R.R., 2004. Estimating fault stability and sustainable fluid pressures for underground storage of CO2 in porous rock. Energy 29, 1445–1456.

Tenthorey, E., Vidal-Gilbert, S., Backe, G., Puspitasari, R., Pallikathekathil, Z.J., Maney, B., Dewhurst, D., 2013. Modelling the geomechanics of gas storage: a case study from the Iona gas field, Australia. Int. J. Greenh. Gas Control 13, 138–148.

Verdon, J.P., Kendall, J.M., Stork, A.L., Chadwick, R.A., White, D.J., Bissell, R.C., 2013. Comparison of geomechanical deformation induced by megatonne-scale CO2 storage at Sleipner,Weyburn, and in Salah. Proc. Natl. Acad. Sci. 110, E2762–E2771.

Vidal-Gilbert, S., Tenthorey, E., Dewhurst, D., Ennis-King, J., Van Ruth, P., Hillis, R., 2010. Geomechanical analysis of the Naylor field, Otway basin, Australia: Implications for CO2 injection and storage. Int. J. Greenh. Gas Control 4, 827–839.

Watts, N.L., 1987. Theoretical aspects of cap-rock and fault seals for single-and two-phase hydrocarbon columns. Mar. Petrol. Geol. 4, 274–307.

Whipp, P.S., Jackson, C.L., Gawthorpe, R.L., Dreyer, T., Quinn, D., 2014. Normal fault array evolution above a reactivated rift fabric; a subsurface example from the northern Horda Platform, Norwegian North Sea. Basin Res. 26, 523–549.